Published in final edited form as:
Biomater Sci. 2013 November 1; 1(11): . doi:10.1039/C3BM60129C.

Collagen-Based Substrates with Tunable Strength for Soft Tissue Engineering

Vivek A. Kumar[1,2,3], **Jeffrey M. Caves**[1,2], **Carolyn A. Haller**[1,2], **Erbin Dai**[1], **Liying Li**[1], **Stephanie Grainger**[1,2], and **Elliot L. Chaikof**[1,2,3]

[1]Department of Surgery, Beth Israel Deaconess Medical Center, Harvard Medical School, Boston, MA 02215

[2]Wyss Institute of Biologically Inspired Engineering of Harvard University, Boston, MA 02215

[3]Department of Biomedical Engineering, Georgia Institute of Technology/Emory University, Atlanta, GA 30332

Abstract

Through the use of mechanical reinforcement of collagen matrices, mechanically strong and compliant 3D tissue mimetic scaffolds can be generated that act as scaffolds for soft tissue engineering. Collagen has been widely used for the development of materials for repair, augmentation or replacement of damaged or diseased tissue. Herein we describe a facile method for the layer-by-layer fabrication of robust planar collagen fiber constructs. Collagen gels cast in a phosphate buffer were dried to form dense collagen mats. Subsequent gels were layered and dried atop mats to create multilayer constructs possessing a range of tunable strengths (0.5 - 11 MPa) and stiffness (1 - 115 MPa). Depending on processing conditions and crosslinking of constructs, strain to failure ranged between 9 to 48%. Collagen mats were constructed into hernia patches that prevented hernia recurrence in Wistar rats.

Keywords

Collagen; mechanical properties; reinforcement; hernia patch; soft tissue

Introduction

One of the common uses for materials in medicine is for surgical wound closure in the treatment of hernias. Hernia repair is known to be the most commonly performed general surgical procedure in the United States accounting for over a million procedures per annum [1]. Current treatment includes primary closure of the fascia surrounding the abdominal wall defect tissue with or without the use of mesh and associated relaxing fascial incisions to achieve tension-free wound closure. Typically, mesh placement is preferred as it results in lower reherniation rates [2]. A variety of synthetic polymeric materials (polypropylene, polyethyleneterephathalate, polytetrafluoroethylene) [3] or decellularized matrices have been used for abdominal wall repair [4]. Patients treated with these materials often suffer from reherniation due to failure at the material-tissue interface or in the case of bioprosthetic matrices of the material itself, infection due to surgical site or implant contamination, seroma formation and general discomfort due to a biomechanical mismatch between the implant and host tissue [3-9]. Several strategies have been employed for the development of

*Address correspondence to: Elliot L. Chaikof, M.D., Ph.D., 110 Francis St, Suite 9F, Boston, MA 02215, Tel: (617) 632-9581, echaikof@bidmc.harvard.edu.

a surgical mesh and other soft tissue replacements that enhance biointegration with host tissue, minimize risk of infection, and improve patient comfort [10].

The generation of scalable mechanically matched and biocompatible materials comprised of native or recombinant structural proteins for soft tissue engineering remains a critical challenge [11]. Synthetic non-degradable and biodegradable polymers that recapitulate the nanofibrous architecture typical of the ECM environment have been widely attempted [12-16]. Concerns over immune rejection, macrophage or neutrophil mediated degradation, chronic inflammation, mechanical failure, and the capacity of these matrices to be integrated into the host system remain significant hurdles. Decellularization of native tissue matrices has been studied as an alternative to the generation of ECM-mimetic scaffolds [17-19]. Given that decellularized tissues are often derived from non-human sources, the presence of residual xenoantigens, as well as the potential for viral or bacterial transmission exists. Decellularized scaffolds have been studied as a niche for host cell infiltration. However, subtle structural and biochemical damage to decellularized matrices can occur during processing. Decellularized tissues are often crosslinked to maintain stability and mechanical integrity, but the ability to truly tailor mechanical properties of such matrices remains limited.

To address these challenges, we have designed a bottom-up approach for the creation of bioartificial matrices for soft tissue applications, and particularly for hernia repair. We hypothesize that the use of reconstituted collagen with specific hierarchical structure and organization afforded by our fabrication technique will better mimic the structure and mechanics of native tissue by providing a more homogeneous and controlled system than decellularized matrices. Further, we show that systematically controlling collagen gel hydration and global micro- and macrostructure, strong collagen sheets can be developed with tunable mechanical properties. Similar reports have noted the diffusivity of collagen films [20], the strength of rolled films [21], the influence of cyclic loading and collagen fibril diameter [22-24] on matrix strength. We have built upon these technologies through a process of layer-by-layer collagen sheet lamination and dehydration. This has yielded matrices that mimic native tissue in nanofibrous structure, mechanical integrity, and biological response, complementing prior studies [21, 22]. Evaluation of collagen matrices in a rat ventral hernia repair model demonstrates the utility of such matrices and their reintegration into host tissue, resolution of inflammatory response, and angiogenesis over a 3-month period.

Experimental Methods

Isolation and purification of monomeric collagen

Monomeric Type I rat tail tendon collagen was obtained by acid extraction from Sprague-Dawley rats (Pel-Freez Biologicals, Rogers, AR) following a procedure adapted from Silver and Trelstad [25]. Briefly, rat tail tendons were extracted with the aid of autoclaved pliers and dissolved in 10 mM HCl for 4 h at 25°C to dissolve the proteinaceous components. Insoluble tissue and other contaminants were removed by centrifugation at 30,000 g at 4°C for 30 min with subsequent vacuum filtration through 20 μm, 0.45 μm, and 0.2 μm filters. The sterile filtered collagen in HCl was precipitated from solution by adding NaCl to a final concentration of 0.7 M. The precipitated collagen was pelleted by centrifugation, redissolved in 10 mM HCl, and dialyzed against 20 mM phosphate buffer at room temperature and then at 4°C, followed by 10 mM HCl at 4°C and deionized water at 4°C. The collagen was then frozen and lyophilized until used.

Production of collagen fiber mats

Monomeric rat tail tendon collagen dissolved in 10 mM HCl (0.625 - 2.5 mg/mL) and neutralized using a gelation buffer (GB, 4.14 mg/mL monobasic sodium phosphate, 12.1 mg/mL dibasic sodium phosphate, 6.86 mg/mL TES (N-tris (hydroxymethyl) methyl-2-aminoethane sulfonic acid sodium salt, 7.89 mg/mL sodium chloride, pH 8.0) at 4°C in rectangular molds (10 × 7 × 0.4 cm) for 24 h. Gels were subsequently placed in a fiber incubation buffer (FIB, 7.89 mg/mL sodium chloride, 4.26 mg/mL dibasic sodium phosphate, 10 mM Tris, pH 7.4) at 37°C for 48 h to promote fibrillogenesis [26]. Individual gels were washed in 2 L of deionized water for 6 hr with 3 changes to remove salts. Gels were then dried at room temperature under a steady air stream to create collagen mats. Stacked mats consisting up to four layers were generated by serially drying additional gels on top of dried mats. Some specimens were crosslinked in genipin (Wako Chemicals USA, Richmond, VA) at 6 mg/mL in PBS at 37°C for 24 h. The density of these mats was determined by lyophilizing and weighing 1 × 1 cm squares for each crosslinking and layering configuration (n = 8/group).

Imaging of composite architecture

Optical, fluorescence, scanning electron (SEM), and transmission electron microscopy (TEM) were used to analyze mat and collagen structure. For SEM studies, dry collagen mats were hydrated in water for 24 h and dehydrated in serial exchanges of ethanol-water mixtures from 30%-100%. The samples were then critical point dried (Auto Samdri 815 Series A, Tousimis, Rockville, MD), sputter coated with 8 nm of gold (208HR Cressington, Watford, England) and imaged at an accelerating voltage of 10,000 eV using a field emission scanning electron microscope (Zeiss Supra 55 FE-SEM, Peabody, MA). Collagen fibril diameters were determined by measuring the diameters of at least 8 fibrils in eight separate 50,000× magnification images for each concentration and crosslinking condition. To determine the presence of D-periodicity, hydrated samples were prepared for TEM. Samples in PBS were washed in 0.1 M cacodylate buffer and fixed in glutaraldehyde. After washing in water, samples were partially dehydrated in ethanol and stained with uranyl acetate. Samples were then dehydrated in ethanol, embedded in resin, and polymerized. Ultrathin (60 - 80 nm) sections were cut using a RMC MT-7000 ultramicrotome (Boeckeler, Tucson, AZ). Post-staining with uranyl acetate and lead citrate was followed by imaging using a JOEL JEM-1400 TEM (JOEL, Tokyo, Japan) at 90,000 V.

Mechanical testing of composites

Collagen sheets were cut using a dog-bone press to yield samples with a gauge length of 13 mm and 4.5 mm width. Samples were mounted onto a Dynamic Mechanical Thermal Analyzer V (DMTA V, Rheometric Scientific, Piscataway, NJ) and immersed in PBS at 37°C. Samples were preconditioned 15 times to 66% of the average maximum failure strain determined from pilot samples and then tested to failure at 5 mm/min (n = 4/group). Hydrated thickness was measured using optical microscopy for calculation of cross-sectional area. Young's modulus was determined from the slope of the last 4% of the stress-strain curve, to allow comparison to published studies.

Ventral hernia repair model

Layered collagen mats were used to repair a ventral hernia using a rat animal model [27]. Abdominal wall defects were created in 225-250 g female Wistar rats and repaired with collagen mats or a commercially available decellularized porcine dermal matrix crosslinked with hexamethylene diisocyanate (HMDI) control implant (1 mm thick Permacol™, Covidien, Mansfield, MA). All studies were approved by the Beth Israel Deaconess Medical Center Institutional Animals Care and Use Committee. Rats were anesthetized using

isoflurane (2.5% induction, 1.5% maintenance); a 5 cm midline incision was made between the xyphoid and pubis. The skin was separated from the muscle layers and a 2.5 cm × 1.5 cm incision was made through the muscle layers to the peritoneum. The patch was placed over the defect and sutured in place using 6-0 Prolene™ suture. A 1 cm long relaxing fascial incision was made 1 cm lateral to either side of the abdominal defect. The skin was closed, and animals were administered pain medication for 48 hr.

Animals were sacrificed at 1, 2, and 3 months, the adhesions between the skin and the implant were noted and changes in implant size measured by photographic analysis. 5 rats were used for each group (Permacol™ or collagen) per timepoint. Harvested samples were removed along with adjacent tissue and fixed in 10% buffered formalin for 24 hours prior to processing. Samples were embedded in paraffin, 5 μm sections obtained and stained for infiltrating cells (Hemotoxylin & Eosin), extracellular matrix production (Masson's Trichrome), monocyte / macrophages (CD68) and endothelial cells, EC, (vWF) (Abcam, Cambridge, MA). Monocyte / macrophage infiltration was measured by counting positively stained nuclei in 6 random fields for 6 samples at each time point. To measure the strength of integration, 4 × 20 mm strips of patch and adjacent tissue were excised and mounted on opposing platens of a uniaxial tensile tester (DMTA V, Rheometric Scientific, Piscataway, NJ) and failure tension determined. Implant area changes were measured from photographs of implants prior to closing and at explantation. Briefly, photographs were taken, as in Figure 8, the outlines of the implant and explant traced in Image J (NIH, Bethesda, Maryland), and compared for each animal.

Statistical Analysis

Mean values and standard deviation was obtained for all measurements, image analyses and mechanical data. Comparisons were performed using the Student's *t* test for unpaired data, ANOVA for multiple comparisons, and Tukey post hoc analysis for parametric data. Nonparametric tests were carried out using the Kruskal-Wallis ANOVA, with Dunn's post hoc analysis as indicated. Values of $p < 0.05$ were considered statistically significant.

Results

Fibrillar microstructure and preservation of native collagen structure

Layer-by-layer collagen networks were produced and both ultrastructure and mechanical properties analyzed (Fig. 1). No distinguishable interface (Fig. 2 A, D) or delamination between layers was observed. Likewise, efforts to peel off individual layers were unsuccessful. Signifcantly, we observed that multilayered constructs displayed a higher density than measured for a single layered film (205 ± 9.35 vs. 268 ± 12.6 mg/cm^3, $p < 0.01$).

Collagen fibril structure was observed using high magnification, 50,000×, SEM images, (Fig. 2 B, C). We observed no significant difference in fibril diameter with collagen concentration (83.1 ± 9.44 nm (2.5 mg/mL gels), 75.7 ± 14.8 nm (1.25 mg/mL gels), 74.3 ± 11.4 nm (0.625 mg/mL gels). TEM confirmed the presence of a D-periodic, 67 nm collagen banding pattern (Fig. 2 E, F).

Mechanically tunable collagen mats as a function of concentration, thickness, and layering

Representative stress-strain curves show the mechanical response of uncrosslinked and crosslink collagen matrices (Fig. 3). Collagen concentration did not influence ultimate tensile strength (~0.7 MPa), stiffness (~2.0 MPa) or strain to failure (~45%) for either uncrosslinked or crosslinked multilayer constructs. Genipin crosslinking produced a substantial significant increase in tensile strength (~5.0 MPa), stiffness (~60 MPa), with a

concomitant decrease in strain at failure (~12 %) (Fig. 3, 6, 7; $p < 0.01$ for comparisons of strength, stiffness and strain to failure). When compared to single layer matrices, multilayer matrices showed an unanticipated increase in strength, from 0.7 to 1.5 MPa and from 5 to 8 MPa for uncrosslinked and crosslinked matrices, respectively (Fig. 4 A, D). A similar trend was noted for stiffness. This effect was observed for mats produced from a variety of collagen concentrations. Single layer collagen mats had a nominal thickness of 10.5 ± 1.7 to 76.4 ± 5.2 μm depending on initial casting collagen concentration (Fig. 6, 7). Of note, laminated collagen gels afforded a decrease in thickness per layer, which was not influenced by the number of collagen layers ($p < 0.01$, Fig. 4, 5).

For animal studies, a 12 layer collagen mat, which was 368 ± 16.5 μm in thickness was produced. Mechanical properties included an ultimate tensile strength of 1.77 ± 0.32 MPa, strain to failure of 34.4 ± 3.4%, Young's Modulus of 6.18 ± 1.45 MPa (Table 1).

Ventral Hernia Model

A ventral hernia model was created by dissecting the abdominal wall between the xyphoid and pubis to the peritoneum, n =5/ timepoint/group (Fig. 8 A). Multilayer collagen patches or Permacol™ patches, as a reference material, were implanted using an overlay technique. Neither patch type was associated with reherniation at time points of up to 3 months (Fig. 8 E). Since the peritoneum was left intact in these studies, no appreciable adhesion to viscera was noted. Comparison of measurements of implant area with area of explant at each time point showed that both multilayer collagen and control patches showed an increase in area at 3 months (collagen 169 ± 26 %, Permacol™ 161 ± 16 %, NS). Initial explantation at 1 month showed minimal degradation of either multilayer collagen or control patches (Fig. 8 C, G). Conversely, multilayer collagen patches showed a higher level of degradation at 2 and 3 months as compared to Permacol™ (Fig. 8 D, H). Tensile strength at the host-patch junction was not significantly different between material types (multilayer collagen: 1 month 1.05 ± 0.24 Nm, 2 month 0.96 ± 0.29 Nm, 3 month 0.98 ± 0.11 Nm; Permacol™: 1 month 1.23 ± 0.32 Nm, 2 month 0.84 ± 0.20 Nm, 3 month 1.03 ± 0.19 Nm).

Histologic evaluation was performed using Masson's Trichrome staining (Fig. 9). Prior to implantation, engineered multilayer collagen matrix and Permacol™ matrix showed distinct morphological features. Abdominal muscle stained red and was present adjacent to highly cellularized peritoneal membrane with neo-tissue formation above and below all implants. After the 3-month implant period, ECM staining of collagen showed distinct morphologic differences compared to earlier time points indicating that the multilayer collagen implant had largely been replaced by new collagen deposition (Fig. 9 B-D). In contrast, the histomorphology of Permacol™ implants was relatively unchanged over the 3-month implant period (Fig. 9 F-H). vWF staining confirmed the development of blood vessels as early as 1 month in both implants (Fig. 10 A, B, E, F). CD68 staining revealed a reduction in monocyte / macrophage infiltration during the 3 month time frame, with a greater reduction observed for the multilayer collagen implants as compared to Permacol™ (38.7 ± 8.4 % vs. 23.7 ± 5.9 %, $p<0.05$) (Fig. 10 C, D, G, H).

Discussion

Dependence of gelation conditions on ultrastructure of collagen gels

Collagen gelation kinetics is highly dependent on collagen isolation method, initial collagen concentration, temperature of gelation, pH and presence of ions. Several groups have shown the effects of the aforementioned parameters on fibrillar size and microarchitecture of collagen matrices [26, 28-32]. Pepsin digested collagen structures are devoid of telopeptide sequences that are critical to fibril formation with recapitulation of native collagen D-

periodic structure, unlike acid solubilized collagen, which still retains telopeptide sequences. Prior reports have noted the effect of longer gelation times and lower initial collagen concentrations allow more time for fibrillogenesis without spatial restrictions from adjacent fibrils [33-38]. Our studies indicate that using our gelation conditions and fabrication technique no significant difference in fibril diameter as a function of concentration (0.625 - 5.0 mg/mL) was noted and did not directly translate to larger scale mechanical differences in ultimate tensile strength or strain at failure of centimeter scale constructs. Recapitulation of D-periodicity in collagen fibrils, as exemplified by the 67 nm banding pattern (Fig. 2 D-F) suggests preservation of cell binding moieties, such as GFOGER that mediate binding to cell surface integrins [39-41].

Use of purified and reconstituted collagen to mimic the extracellular matrix

The extracellular matrix is composed of several components that provide strength, structural support, and cell adhesion. Recapitulation of the nanofibrous ECM milieu has been attempted using a variety of technologies – electrospinning [42, 43], nanofibrous scaffolds [44] and use of naturally derived, reconstituted matrices [45]. However, several drawbacks limit the use of these biomaterials, including denaturation of electrospun proteins, residual pro-inflammatory constituents in decellularized allogeneic or xenogeneic derived scaffolds, undesirable biodegradation products. Further the inability to tune the mechanical properties to match those of native tissue limits the application of such materials. The desirability of collagen as a biomaterial is supported by the its capacity to form a fibrillar nanofibrous structure capable of supporting cell adhesion, proliferation, and differentiation, a high level of species homology, and FDA approval of several collagen based products. However, to date, a major limitation of collagen-based tissue engineering is the inability to modulate the mechanics, strength, and suturability of relatively weak collagen scaffolds.

Tunable ECM mimetics with enhanced mechanical properties

The present study noted the effect of a variety of processing techniques, such as initial gel concentration; layering of collagen matrices, and crosslinking on the ultimate tensile strength, strain at failure, Young's Modulus, and film thickness. Mechanical testing of hydrated collagen mats showed that concentration did not afford increased ultimate tensile strength or stiffness for mats. Since ultimate tensile strength is the failure stress divided by cross-sectional area, increasing collagen mass in constructs with commensurate increase in thickness did yield significantly different mechanical strengths (Figs. 6, 7). However, stacking of collagen layers led to an unanticipated increase in the ultimate tensile strength, which may be due to an apparent structural reinforcement of collagen matrices when layered as a result of an integration of layers leading to a buttressed fibrillar microstructure. We observed that during mechanical testing, failure of matrices occurred through transverse fracture in the direction perpendicular to axial stretch, without delamination of collagen layers. Additionally, layered structures were associated with a reduction in layer thickness as compared to single layer mats, further suggesting the integration of collagen fibrils between layers afforded an interwoven structure. This was corroborated by the observation of a step-wise increase in density. While there was an increase in ultimate tensile strength and stiffness, there was no increase in strain to failure upon layering of collagen mats. Collagen fibrils from adjacent layers likely form a localized interpenetrating network at each interface, resulting in higher ultimate tensile strengths [46-51]. Coupled with the milieu of hydroxyl and sulfhydryl groups in collagen, micro-crosslinks, both physical and chemical (Van der Waal's, ester, thioester) may form during gel dehydration, which has been shown to enhance ultimate tensile strength of collagen matrices [52-55].

The capacity to crosslink collagen constructs allows for the generation of mechanically tunable structures with mechanical properties in the range of those observed for blood

vessels, cartilage, tendon, abdominal wall defect replacements or artificial skin [56-58]. In this investigation, genipin, a naturally occurring crosslinker with improved biocompatibility as compared to glutaraldehyde, was used to crosslink lysine residues [59-61]. Genipin crosslinking increased ultimate tensile strength and stiffness, Young's modulus, with limited change in strain at failure.

Synthetic hernia meshes are strong plastic materials that are often stiffer than native abdominal wall fascial tissue and potentially cause increased patient discomfort [62]. Conversely, the designed multilayer uncrosslinked collagen matrix has more suitable mechanical properties that can be easily tuned based on fabrication conditions (Table 1). These uncrosslinked collagen matrices showed similar ultimate tensile strengths, strains and stiffness to a variety of biologically derived meshes and native tissue [63] including, Permacol™, SIS, native linea alba and abdominal wall fascia [27, 62, 64-66]. Subsequent to implantation, an important metric in determining mechanical robustness of meshes is strength of integration with surrounding tissue. This report has shown that multilayer collagen matrices have strength of integration similar to that of commercially available meshes: Permacol™, AlloDerm™, Surgisis™ and Vicryl™ woven mesh [67, 68].

Biocompatible, dense fibrillar matrices support tissue ingrowth and remodeling

Dense collagen matrices are currently being investigated for a variety of tissue engineering applications within our laboratory including development of microvasculature, small diameter vascular grafts, and soft tissue mimics as demonstrated in this study. Layering of collagen matrices substantially enhanced mechanical properties, such as ultimate tensile strength and stiffness. For comparison to commercially available wound closure products, Permacol, a decellularized porcine dermal matrix crosslinked with hexamethylene diisocyanate (HMDI), was used as a reference material. Engineered multilayer collagen matrices were 65% thinner than the 1 mm thick Permacol™ matrices. This may have contributed to the faster degradation and remodeling of collagen matrices over the 3 month study period compared to Permacol™ matrices. Differences in the rates of patch replacement may also be attributable to differences in crosslinking of Permacol™ in HMDI [69, 70]. The presence of HMDI or residual xenoantigens may also have prolonged the $CD68^+$ inflammatory response in Permacol™ matrices [69, 70]. Neither patch material showed a predilection for infection, seroma formation, or mechanical failure. These factors suggest utility of this new construct for hernia repair and further large animal studies are warranted.

The fabrication scheme outlined herein allows for the introduction of a variety of additional factors that may enhance wound healing and prevent infection [6]. The casting of hydrogels and the layer-by-layer stacking technique allows localized incorporation of small molecule drugs or cells which can potentially reduce the risk of common complications associated with hernia repair [5, 7]. As such, future studies will aim to evaluate collagen matrices in surgically infected fields, loading of cells and small molecule drugs to influence the inflammatory environment and potential strategies for enhanced tissue repair.

Conclusions

Collagen use in biomaterials dates back several decades. Specific to tissue engineering scaffolds, collagen matrices developed in this study have ultimate tensile strengths that approximate or exceed that of native soft tissue, and, to our knowledge, is the first report of a well characterized lamellae that can be manipulated for use in a wide variety of applications. We have shown an unexpected increase in ultimate tensile strength and stiffness of matrices with tunable mechanical properties over several orders of magnitude and preservation of native fibrillar, D-periodic structure. Finally an in vivo model of ventral

hernia repair, shows the ability of dense collagen matrices to rapidly re-integrate with host tissue, neotissue formation, reduction in number of inflammatory cells, development of nascent blood vessels and maintenance of strength – prohibiting reherniation. These results have provided impetus for studies in larger animal models. The biointegration potential of these thin strong collagen fabrics, coupled with their muted inflammatory potential support their use for a variety of other applications currently under investigation.

Acknowledgments

Electron microscopy was performed at the Center for Nanoscale Systems at Harvard University, and the Wyss Institute of Biologically Inspired Design. This project was supported by NIH R01 HL083867, RO1HL60464, and RO1HL71336.

References

1. Rutkow IM. Surg Clin North Am. 2003; 83:1045–1051. [PubMed: 14533902]
2. Luijendijk RW, Hop WC, van den Tol MP, de Lange DC, Braaksma MM, JN IJ, Boelhouwer RU, de Vries BC, Salu MK, Wereldsma JC, Bruijninckx CM, Jeekel J. N Engl J Med. 2000; 343:392–398. [PubMed: 10933738]
3. Earle DB, Mark LA. Surg Clin North Am. 2008; 88:179–201. [PubMed: 18267169]
4. Smart NJ, Marshall M, Daniels IR. Surgeon. 2012; 10:159–171. [PubMed: 22436406]
5. Anthony T, Bergen PC, Kim LT, Henderson M, Fahey T, Rege RV, Turnage RH. World J Surg. 2000; 24:95–100. [PubMed: 10594211]
6. Hiles M, Record Ritchie RD, Altizer AM. Surg Innov. 2009; 16:26–37. [PubMed: 19223383]
7. White TJ, Santos MC, Thompson JS. Am Surg. 1998; 64:276–280. [PubMed: 9520825]
8. DuBay DA, Wang X, Adamson B, Kuzon WM Jr, Dennis RG, Franz MG. Surgery. 2006; 140:14–24. [PubMed: 16857438]
9. Dunne JR, Malone DL, Tracy JK, Napolitano LM. J Surg Res. 2003; 111:78–84. [PubMed: 12842451]
10. Cevasco M, Itani KM. Surg Infect (Larchmt). 2012; 13:209–215. [PubMed: 22913337]
11. Place ES, Evans ND, Stevens MM. Nat Mater. 2009; 8:457–470. [PubMed: 19458646]
12. Yang J, Motlagh D, Webb AR, Ameer GA. Tissue Eng. 2005; 11:1876–1886. [PubMed: 16411834]
13. Salerno A, Oliviero M, Di Maio E, Iannace S, Netti PA. J Mater Sci Mater Med. 2009; 20:2043–2051. [PubMed: 19430895]
14. Gercek I, Tigli RS, Gumusderelioglu M. J Biomed Mater Res A. 2008; 86:1012–1022. [PubMed: 18067167]
15. Chew SY, Wen Y, Dzenis Y, Leong KW. Curr Pharm Des. 2006; 12:4751–4770. [PubMed: 17168776]
16. Sachlos E, Czernuszka JT. Eur Cell Mater. 2003; 5:29–39. [PubMed: 14562270]
17. Badylak SF, Nerem RM. Proc Natl Acad Sci U S A. 2010; 107:3285–3286. [PubMed: 20181571]
18. Badylak SF, Freytes DO, Gilbert TW. Acta Biomater. 2009; 5:1–13. [PubMed: 18938117]
19. Badylak SF. Biomaterials. 2007; 28:3587–3593. [PubMed: 17524477]
20. Ho HO, Lin CW, Sheu MT. J Control Release. 2001; 77:97–105. [PubMed: 11689263]
21. Brown RA, Wiseman M, Chuo CB, Cheema U, Nazhat SN. Advanced Functional Materials. 2005; 15:1762–1770.
22. Cheema U, Chuo CB, Sarathchandra P, Nazhat SN, Brown RA. Advanced Functional Materials. 2007; 17:2426–2431.
23. Cheema U, Chuo CB, Sarathchandra P, Nazhat SN, Brown RA. Tissue Engineering. 2007; 13:1688–1688.
24. Abou Neel EA, Cheema U, Knowles JC, Brown RA, Nazhat SN. Soft Matter. 2006; 2:986–992.
25. Silver FH, Trelstad RL. J Biol Chem. 1980; 255:9427–9433. [PubMed: 7410433]

26. Pins GD, Christiansen DL, Patel R, Silver FH. Biophys J. 1997; 73:2164–2172. [PubMed: 9336212]
27. Caves JM, Cui W, Wen J, Kumar VA, Haller CA, Chaikof EL. Biomaterials. 2011; 32:5371–5379. [PubMed: 21550111]
28. Wood GC, Keech MK. Biochem J. 1960; 75:588–598. [PubMed: 13845809]
29. Reed R, Wood MJ, Keech MK. Nature. 1956; 177:697–699. [PubMed: 13321936]
30. San Antonio JD, Lander AD, Karnovsky MJ, Slayter HS. J Cell Biol. 1994; 125:1179–1188. [PubMed: 8195298]
31. Stamov D, Grimmer M, Salchert K, Pompe T, Werner C. Biomaterials. 2008; 29:1–14. [PubMed: 17892897]
32. Paderi JE, Sistiabudi R, Ivanisevic A, Panitch A. Tissue Eng Part A. 2009; 15:2991–2999. [PubMed: 19323607]
33. Forgacs G, Newman SA, Hinner B, Maier CW, Sackmann E. Biophys J. 2003; 84:1272–1280. [PubMed: 12547807]
34. Djabourov M, Lechaire JP, Gaill F. Biorheology. 1993; 30:191–205. [PubMed: 8286722]
35. Achilli M, Lagueux J, Mantovani D. Macromol Biosci. 2010; 10:307–316. [PubMed: 19946859]
36. Raspanti M, Viola M, Sonaggere M, Tira ME, Tenni R. Biomacromolecules. 2007; 8:2087–2091. [PubMed: 17530890]
37. Stuart K, Panitch A. Biomacromolecules. 2009; 10:25–31. [PubMed: 19053290]
38. Stuart K, Panitch A. Biopolymers. 2008; 89:841–851. [PubMed: 18488988]
39. Jokinen J, Dadu E, Nykvist P, Kapyla J, White DJ, Ivaska J, Vehvilainen P, Reunanen H, Larjava H, Hakkinen L, Heino J. J Biol Chem. 2004; 279:31956–31963. [PubMed: 15145957]
40. Heino J, Huhtala M, Kapyla J, Johnson MS. Int J Biochem Cell Biol. 2009; 41:341–348. [PubMed: 18790075]
41. Heino J. Bioessays. 2007; 29:1001–1010. [PubMed: 17876790]
42. Bhardwaj N, Kundu SC. Biotechnol Adv. 2010; 28:325–347. [PubMed: 20100560]
43. Dahlin RL, Kasper FK, Mikos AG. Tissue Eng Part B Rev. 2011; 17:349–364. [PubMed: 21699434]
44. Webb AR, Yang J, Ameer GA. Expert Opin Biol Ther. 2004; 4:801–812. [PubMed: 15174963]
45. Hoshiba T, Lu H, Kawazoe N, Chen G. Expert Opin Biol Ther. 2010; 10:1717–1728. [PubMed: 21058932]
46. Yang L, van der Werf KO, Koopman BF, Subramaniam V, Bennink ML, Dijkstra PJ, Feijen J. J Biomed Mater Res A. 2007; 82:160–168. [PubMed: 17269147]
47. van der Rijt JA, van der Werf KO, Bennink ML, Dijkstra PJ, Feijen J. Macromol Biosci. 2006; 6:697–702. [PubMed: 16967482]
48. Wang X, Li X, Yost MJ. J Biomed Mater Res A. 2005; 74:263–268. [PubMed: 15962267]
49. Cornwell KG, Lei P, Andreadis ST, Pins GD. J Biomed Mater Res A. 2007; 80:362–371. [PubMed: 17001644]
50. Caves JM, Kumar VA, Wen J, Cui W, Martinez A, Apkarian R, Coats JE, Berland K, Chaikof EL. J Biomed Mater Res B Appl Biomater. 2010; 93:24–38. [PubMed: 20024969]
51. Fantner GE, Hassenkam T, Kindt JH, Weaver JC, Birkedal H, Pechenik L, Cutroni JA, Cidade GA, Stucky GD, Morse DE, Hansma PK. Nat Mater. 2005; 4:612–616. [PubMed: 16025123]
52. Sallach RE, Cui W, Wen J, Martinez A, Conticello VP, Chaikof EL. Biomaterials. 2009; 30:409–422. [PubMed: 18954902]
53. Wu X, Sallach RE, Caves JM, Conticello VP, Chaikof EL. Biomacromolecules. 2008; 9:1787–1794. [PubMed: 18558738]
54. Thostenson ET, Ren Z, Chou TW. Composites Sci Tech. 2001; 61:1899–1912.
55. Wagner HD, Vaia RA. Materials Today. 2004; 7:38–42.
56. Kurane A, Simionescu DT, Vyavahare NR. Biomaterials. 2007; 28:2830–2838. [PubMed: 17368531]
57. Yang S, Leong KF, Du Z, Chua CK. Tissue Eng. 2001; 7:679–689. [PubMed: 11749726]
58. Zhang R, Ma PX. J Biomed Mater Res. 2000; 52:430–438. [PubMed: 10951385]

59. Bigi A, Cojazzi G, Panzavolta S, Roveri N, Rubini K. Biomaterials. 2002; 23:4827–4832. [PubMed: 12361622]
60. Sung HW, Huang RN, Huang LL, Tsai CC. J Biomater Sci Polym Ed. 1999; 10:63–78. [PubMed: 10091923]
61. Huang LL, Sung HW, Tsai CC, Huang DM. J Biomed Mater Res. 1998; 42:568–576. [PubMed: 9827681]
62. Brown CN, Finch JG. Ann R Coll Surg Engl. 2010; 92:272–278. [PubMed: 20501011]
63. Hollinsky C, Sandberg S. Clinical Biomechanics. 2007; 22:88–92. [PubMed: 16904247]
64. Song C, Alijani A, Frank T, Hanna GB, Cuschieri A. Surg Endosc. 2006; 20:987–990. [PubMed: 16738998]
65. Pott PP, Schwarz MLR, Gundling R, Nowak K, Hohenberger P, Roessner ED. Plos One. 2012; 7
66. Eberli D, Atala A, Yoo JJ. J Mater Sci Mater Med. 2011; 22:741–751. [PubMed: 21286788]
67. Rice RD, Ayubi FS, Shaub ZJ, Parker DM, Armstrong PJ, Tsai JW. Aesthetic Plastic Surgery. 2010; 34:290–296. [PubMed: 19967358]
68. Mulier KE, Nguyen AH, Delaney JP, Marquez S. Hernia. 2011; 15:315–319. [PubMed: 21234626]
69. de Castro Bras LE, Shurey S, Sibbons PD. Hernia. 2012; 16:77–89. [PubMed: 21805341]
70. Deeken CR, Melman L, Jenkins ED, Greco SC, Frisella MM, Matthews BD. J Am Coll Surg. 2011; 212:880–888. [PubMed: 21435917]

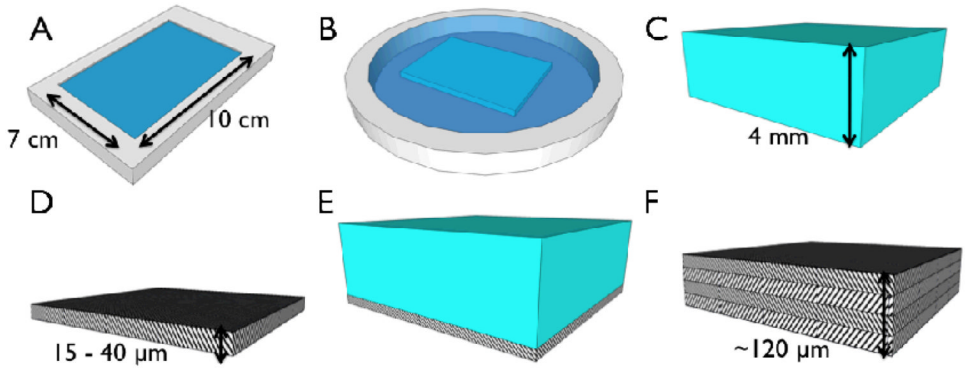

Figure 1.

Schematic of fabrication strategy for layered collagen networks. (**A**) Collagen gels were neutralized in a rectangular mold (10 × 7 × 0.4 cm) in a gelation buffer, GB, at 4°C for 24 h. (**B**) Gels were incubated in fibril incubation buffer, FIB, at 37°C for 48 h. (**C**) 4mm thick gels were washed in DI water, and (**D**) dried to dense micron thick matrices. (**E**) Subsequent gels were dried atop dried matrices to generate multilayer constructs (**F**).

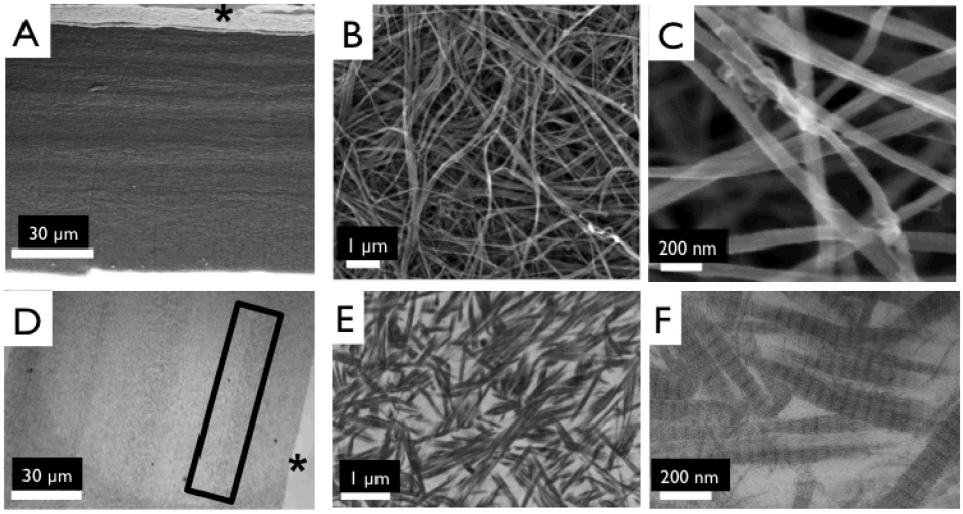

Figure 2.

Ultrastructure of collagen matrices. Scanning electron micrographs of side views of 4 layered collagen matrix (**A**), showing indistinguishable interface between layers, magnified image to show dense fibrillar structure 10,000× (**B**), and 50,000× (**C**). Transmission electron micrographs of 4 layered collagen matrix (**D**), magnified image to show dense fibrillar structure at interface of collagen layers (**E**), and magnified image of a showing D-periodic banding pattern (**F**). *Top of layered construct. Box shows interface region between two collagen layers.

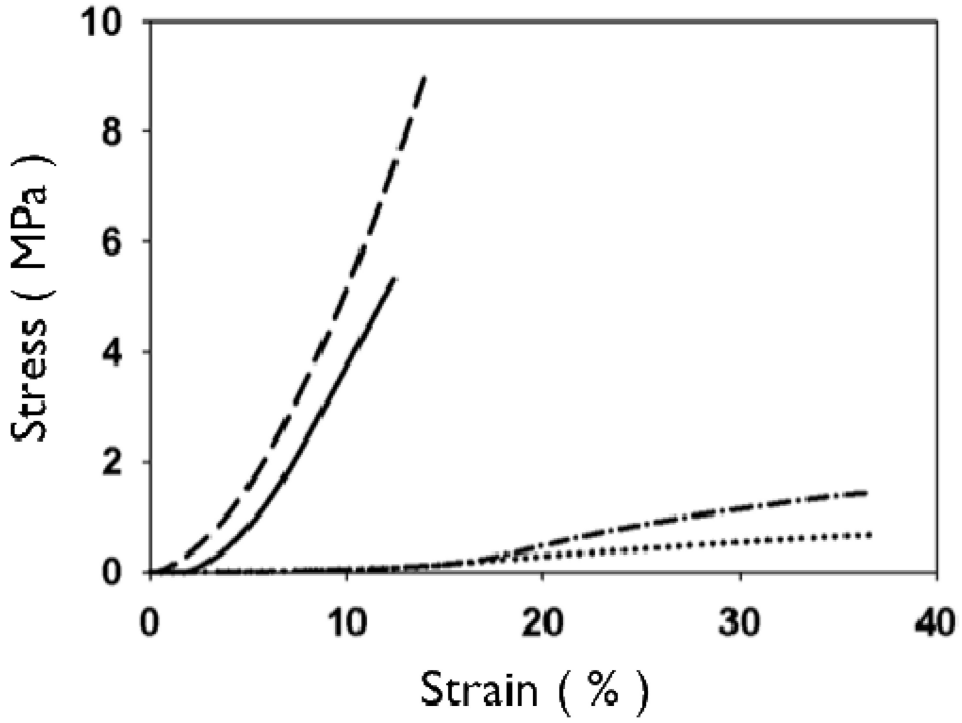

Figure 3.

Representative stress-strain curves of 2.5 mg/mL uncrosslinked and crosslinked collagen networks. Uncrosslinked single layer (dotted line, dash-dot) collagen networks show higher strain at failure and greater extensibility than crosslinked matrices (dashed line, solid line). Layered matrices showed an increase in ultimate tensile strength for both uncrosslinked (single layer: dotted vs. four layer:dash-dot) and crosslinked (single layer: solid vs. four layer: dash) matrices.

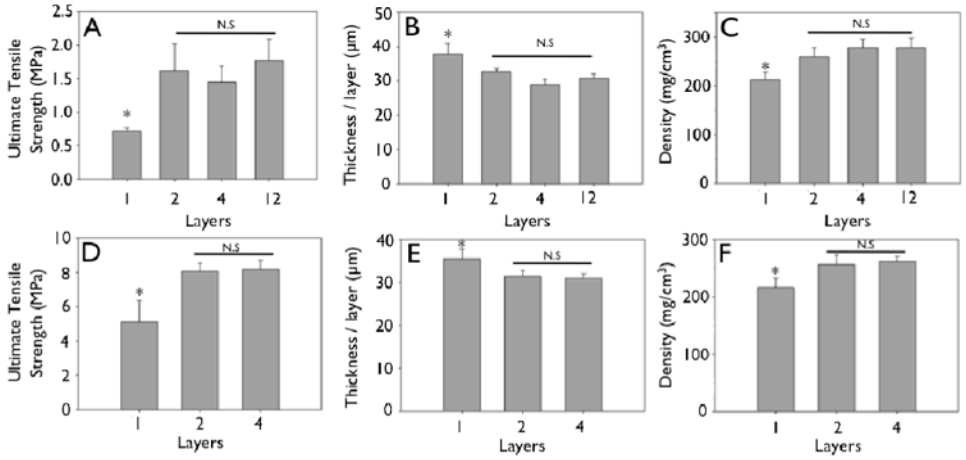

Figure 4.

Mechanical strengthening observed during layering of engineered collagen matrices (collagen concentration 2.5 mg/mL). **A, D**: Ultimate tensile strength of uncrosslinked (**A**) and crosslinked (**D**) engineered collagen matrices as a function of layering. **B, E**: Non-linear decrease in thickness per layer of uncrosslinked (**B**) and crosslinked (**E**) engineered collagen matrices as a function of layering. **C, F**: Non-linear increase in density of engineered collagen matrices of uncrosslinked (**A**) and crosslinked (**D**) engineered collagen matrices as a function of layering (*$p<0.05$).

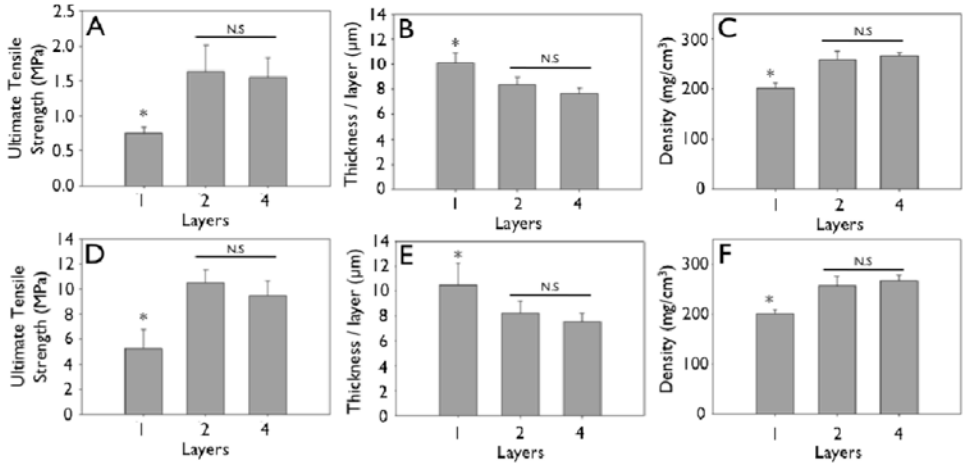

Figure 5.

Mechanical strengthening observed during layering of engineered collagen matrices (collagen concentration 0.625 mg/mL). **A, D**: Ultimate tensile strength of uncrosslinked (**A**) and crosslinked (**D**) engineered collagen matrices as a function of layering. **B, E**: Non-linear decrease in thickness per layer of uncrosslinked (**B**) and crosslinked (**E**) engineered collagen matrices as a function of layering. **C, F**: Non-linear increase in density of engineered collagen matrices of uncrosslinked (**A**) and crosslinked (**D**) engineered collagen matrices as a function of layering.

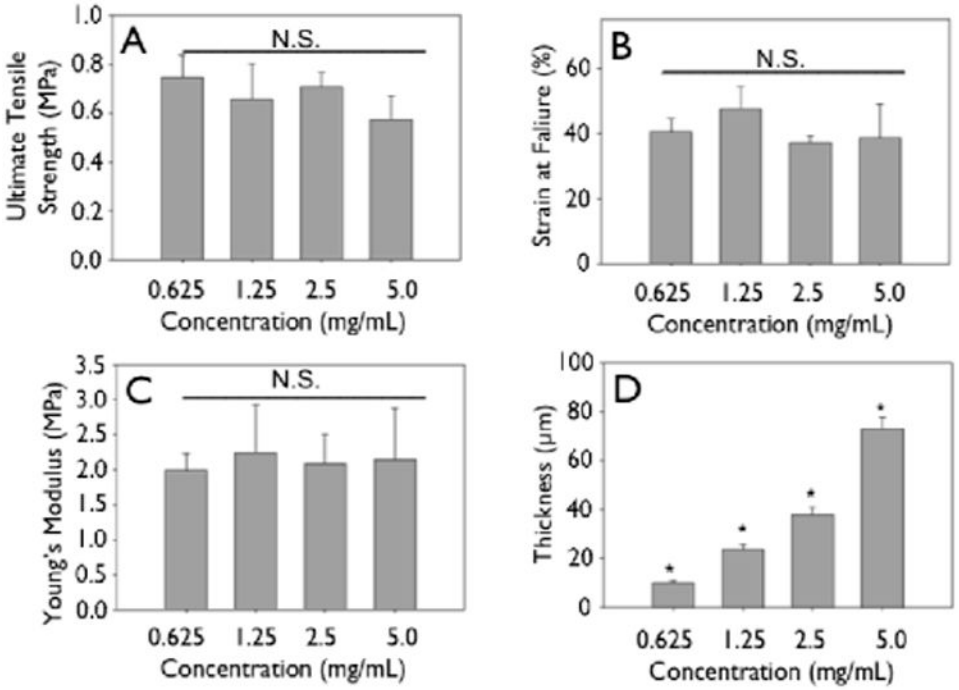

Figure 6.

Mechanics of non-crosslinked engineering collagen matrices as a function of concentration. Gels of different concentrations were cast at 4 mm initial thickness, dried and mechanically tested. (**A**) Ultimate tensile strength, (**B**) strain at failure, (**C**) Young's modulus do not change significantly when concentration of initial constructs is increased. (**D**) Thickness shows a linear increase.

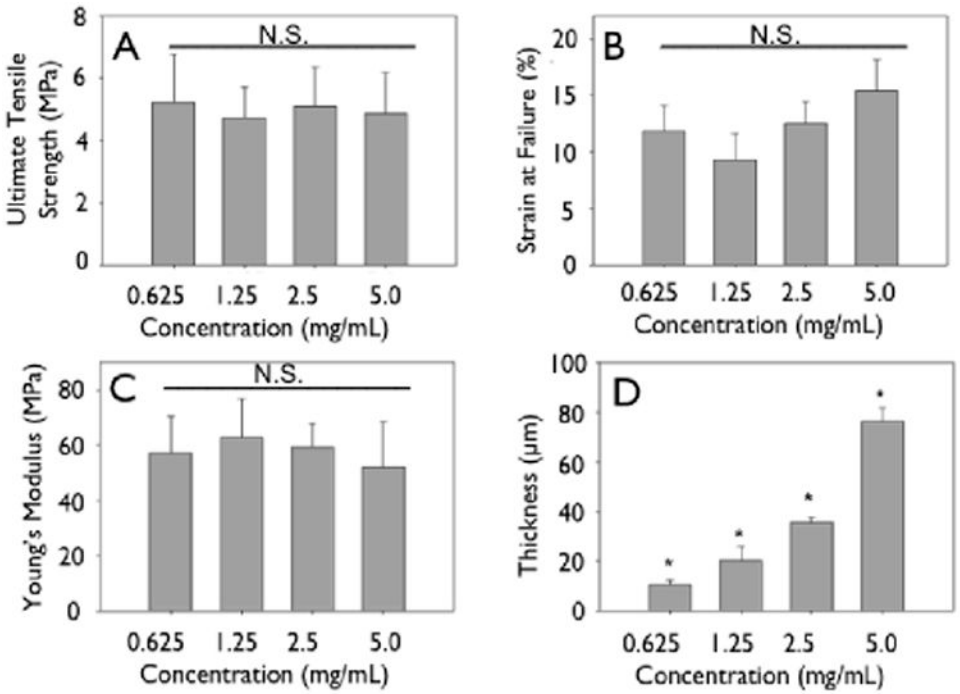

Figure 7.

Mechanics of crosslinked engineered collagen matrices as a function of concentration. Gels of different concentrations were cast at 4 mm initial thickness, dried, crosslinked and mechanically tested. (**A**) Ultimate tensile strength, (**B**) strain at failure, (**C**) Young's modulus do not change significantly when concentration of initial constructs is increased. (**D**) Thickness shows a linear increase.

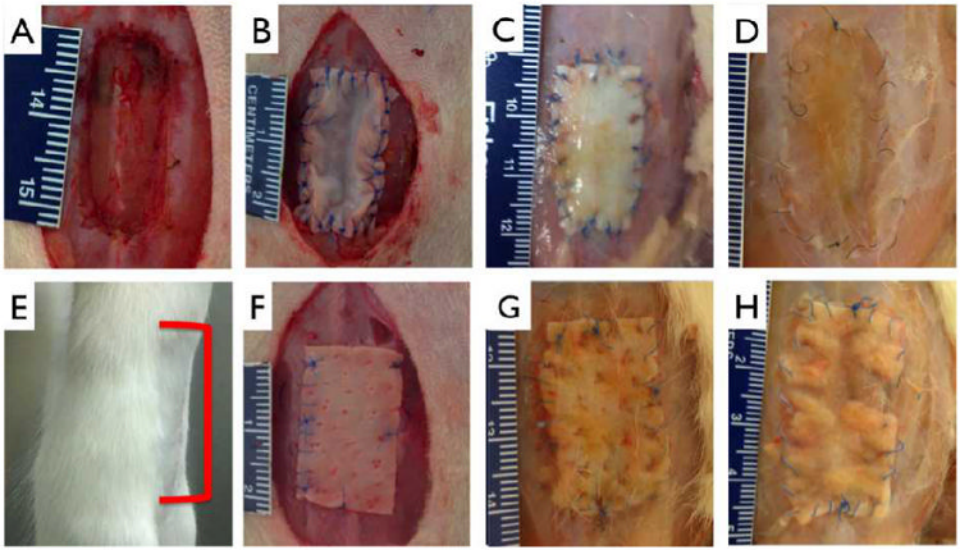

Figure 8.

Abdominal wall model and repair. Incisional hernia model was created by cutting through the abdominal wall to the peritoneum (**A**). Multilayer (12 layered) collagen patch (**B**) or 1 mm thick Permacol™ patch (**F**) was sown into place using 6-0 suture. **E**: Representative image showing none of the treatment or control groups exhibited reherniation at any explant time points, red bracket indicates approximate implant site. Undegraded multilayer collagen (**C**) and Permacol™ (**G**) are clearly present at 1 month. At 3 months, collagen patch shows appreciable reintegration with host tissue (**D**), as compared to control (**H**). Scale bar minor units in mm.

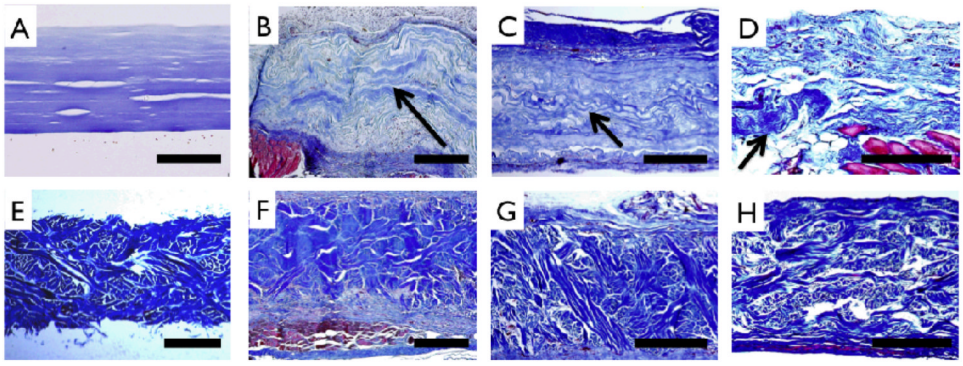

Figure 9.

Extracellular matrix staining (Masson's Trichrome) of unimplanted and implanted samples. Multilayer collagen (**A**) and Permacol™ (**E**) patches prior to implant show uniform thickness and distinct morphology. For multilayer collagen implants, wavy morphology collagen (arrows) is noted above muscle (red) and adjoining highly cellularized peritoneal layer at 1 month (**B**), is clearly delineated in the center of the receullularized implant at 2 months (**C**), and is seen in isolated pockets at 3 months (**D**). Permacol™ implants can be clearly distinguished from host tissue at 1 month (**F**), 2 months (**G**) and 3 months (**H**), resembling preimplant structure and morphology. Scale bar A-D: 200 μm and E-H: 500 μm.

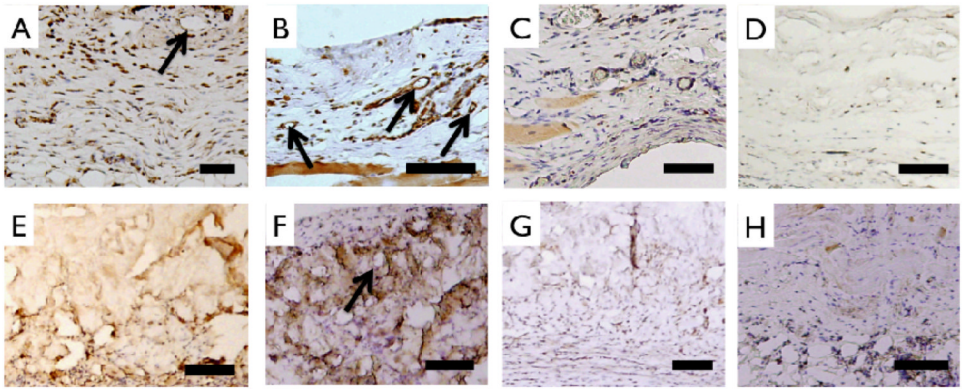

Figure 10.

Staining of cellular infiltrate of implanted samples. Anti-rat vWF staining characterized endothelialization of 1 month collagen (**A**), 3 month collagen (**B**), 1 month control (**E**) and 3 month control (**F**) samples. Arrows point to circular vessel like structures. Monocyte/macrophage marker CD68 staining of 1 month collagen (**C**), 3 month collagen (**D**), 1 month control (**G**) and 3 month control (**H**). Total number of $CD68^{+}$ nuclei decreases more in collagen implants compared to Control implants at 3 months. Scale bar 100 μm.

Table 1

Comprehensive list of tunable mechanical properties of engineered collagen matrices

Design	Collagen Concentration	Crosslinked	Layers	Ultimate Tensile Strength (MPa)	Strain at failure (%)	Young's Modulus (MPa)	Resilience (%)	Thickness (μm)
1	0.625	Yes	1	5.22 ± 1.54	11.8 ± 2.33	57.2 ± 13.2	93.0 ± 3.77	10.5 ± 1.74
2	0.625	Yes	2	10.5 ± 1.07	12.1 ± 2.93	114 ± 15.2	93.1 ± 2.56	16.5 ± 1.93
3	0.625	Yes	4	9.46 ± 1.23	15.6 ± 2.27	94.8 ± 15.8	93.8 ± 3.31	30.2 ± 2.78
4	1.25	Yes	1	4.72 ± 1.01	9.29 ± 2.31	62.8 ± 13.8	96.6 ± 1.36	20.5 ± 5.65
5	2.5	Yes	1	5.11 ± 1.24	12.5 ± 1.91	59.4 ± 8.19	96.1 ± 1.67	35.5 ± 2.26
6	2.5	Yes	2	8.03 ± 0.49	10.8 ± 0.91	106 ± 9.22	97.8 ± 1.26	63.0 ± 2.47
7	2.5	Yes	4	8.17 ± 0.53	13.0 ± 0.96	93.3 ± 4.03	98.6 ± 0.26	124 ± 2.42
8	5	Yes	1	4.86 ± 1.32	15.4 ± 2.73	52.0 ± 16.5	98.7 ± 1.45	76.4 ± 5.21
9	0.625	No	1	0.75 ± 0.09	40.4 ± 4.35	1.99 ± 0.24	57.9 ± 16.7	10.1 ± 0.81
10	0.625	No	2	1.63 ± 0.38	38.9 ± 5.29	6.27 ± 1.57	60.0 ± 12.7	16.8 ± 1.13
11	0.625	No	4	1.55 ± 0.29	38.4 ± 6.35	6.10 ± 0.99	57.7 ± 5.66	30.6 ± 1.87
12	1.25	No	1	0.80 ± 0.11	47.6 ± 6.72	2.24 ± 0.69	73.6 ± 9.50	23.6 ± 1.99
13	2.5	No	1	0.71 ± 0.06	37.1 ± 2.21	2.09 ± 0.42	58.9 ± 4.43	37.8 ± 3.09
14	2.5	No	2	1.62 ± 0.40	36.9 ± 12.5	5.22 ± 0.48	63.9 ± 2.62	65.3 ± 2.01
15	2.5	No	4	1.45 ± 0.23	36.9 ± 3.24	4.48 ± 0.58	61.8 ± 3.65	116 ± 5.69
16	2.5	No	12	1.77 ± 0.32	34.4 ± 3.89	6.18 ± 1.45	67.9 ± 2.30	368 ± 16.5
17	5	No	1	0.57 ± 0.09	38.6 ± 10.3	2.15 ± 0.730	66.7 ± 4.91	73.1 ± 4.56

Data is represented at mean ± S.D. for 4 representative samples.

Biomater Sci. Author manuscript; available in PMC 2014 November 01.